

DNA-nanoparticle superlattices formed from anisotropic building blocks

Matthew R. Jones^{1,2}, Robert J. Macfarlane^{2,3}, Byeongdu Lee⁴, Jian Zhang^{2,3}, Kaylie L. Young^{2,3}, Andrew J. Senesi^{2,3} and Chad A. Mirkin^{1,2,3}★

Directional bonding interactions in solid-state atomic lattices dictate the unique symmetries of atomic crystals, resulting in a diverse and complex assortment of three-dimensional structures that exhibit a wide variety of material properties. Methods to create analogous nanoparticle superlattices are beginning to be realized^{1–5}, but the concept of anisotropy is still largely underdeveloped in most particle assembly schemes⁶. Some examples provide interesting methods to take advantage of anisotropic effects^{7–11}, but most are able to make only small clusters or lattices that are limited in crystallinity and especially in lattice parameter programmability^{12–17}. Anisotropic nanoparticles can be used to impart directional bonding interactions on the nanoscale^{6,18}, both through face-selective functionalization of the particle with recognition elements to introduce the concept of valency^{19–21}, and through anisotropic interactions resulting from particle shape^{13,22}. In this work, we examine the concept of inherent shape-directed crystallization in the context of DNA-mediated nanoparticle assembly. Importantly, we show how the anisotropy of these particles can be used to synthesize one-, two- and three-dimensional structures that cannot be made through the assembly of spherical particles.

Particle assembly is a rapidly developing field of research, because the properties of superlattices can be as different from their individual components as the physical properties of nanoparticles are from bulk materials^{6,14,18}. Shape is an important parameter that affects the properties of a particle, and therefore the incorporation of anisotropic nanostructures into colloidal crystals should lead to materials with as yet undiscovered collective phenomena⁶. Maximum utility of these structures requires that a technique be developed to rationally integrate particles with non-spherical shapes into ordered assemblies. The use of DNA as a ligand for the three-dimensional (3D) crystallization of nanoparticles into colloidal superlattices has many advantages over other assembly techniques^{1–4}. In particular, the synthetically programmable length and recognition properties of DNA have enabled researchers to generate well-defined superlattices from spherical nanoparticles that vary in size (5–80 nm; ref. 23). Moreover, the technique provides nanometre-scale precision in programming the resulting lattice parameters. By replacing the spherical cores that associate through isotropic hybridization interactions with anisotropic nanostructures, we hypothesized that directional bonding interactions could be facilitated by virtue of different particle shapes (Fig. 1a).

Dense DNA functionalization of anisotropic nanostructures (previously demonstrated only for a single anisotropic nanostructure²¹) was achieved through a combination of particle

purification, overgrowth or appropriate surfactant mixtures. These procedures allow one to prepare monodisperse (<10%), pure (>95%) solutions of DNA-functionalized triangular nanoprisms²⁴, nanorods²⁵, rhombic dodecahedra²⁶ and octahedra²⁶ (see Supplementary Information for details of the synthesis and functionalization procedures, Fig. 1b). Nanoparticle assembly occurred through the hybridization of DNA linkers (containing 23, 64, 105, 146 and 187 nucleobases) to the oligonucleotides anchored to the particles (Fig. 1d). On binding to the nanoparticle, these linkers present multiple 'sticky ends' at a programmable distance from the nanoparticle surface, creating, in essence, a controllably sized 'DNA shell' that directs the crystallization process²³. Cooperative melting transitions (where 'melting' refers to the dehybridization of DNA bases linking particles) have been measured for crystals formed in solution for each of these particle shapes, indicating a dense surface coverage of oligonucleotides²⁷, which is essential for the assembly and subsequent crystallization process²³ (Fig. 1c).

Small-angle X-ray scattering (SAXS) was used to interrogate the colloidal crystal structures synthesized from anisotropic particles. SAXS represents a powerful characterization tool for this new class of solution-phase-assembled nanostructures, and can give the symmetries, lattice constants, particle orientation and domain size of a 3D ordered structure without requiring drying of the sample (see Table 1), which significantly affects the resulting lattices²³. Modelling of nanoparticle superlattices has been carried out to corroborate these results by comparing modelled SAXS patterns to those obtained experimentally. Additionally, transmission electron micrographs of several ordered nanoparticle crystals, embedded in a resin, support the conclusions drawn from the SAXS data and have been included in the Supplementary Information.

The first systems examined were assemblies created from primarily 1D structures (nanorods), where a '1D' particle is defined as having a length significantly greater than its width or depth. As has been previously shown with spherical particles, the most stable crystal structure for a given system is typically the one with the largest number of DNA linker interactions³; one would therefore predict that these rods would preferentially assemble with their long axes parallel to each other, to maximize the hybridization events between DNA sticky ends. It is important to note that there is a difference between the processes of particle 'crystallization' and particle 'assembly'. In this context, particle crystallization refers to positioning particles in an ordered formation that has translational symmetry, whereas assembly refers to the process of DNA-hybridization-induced association, regardless of the structure of the aggregate. It has previously been demonstrated that the process of particle assembly occurs on a significantly faster timescale than the process of

¹Department of Materials Science and Engineering, Evanston, Illinois 60208-3113, USA, ²International Institute for Nanotechnology, Northwestern University, 2145 Sheridan Road, Evanston, Illinois 60208-3113, USA, ³Department of Chemistry, Evanston, Illinois 60208-3113, USA, ⁴Advanced Photon Source, Argonne National Laboratory, Argonne, Illinois 60439, USA. *e-mail: chadnano@northwestern.edu.

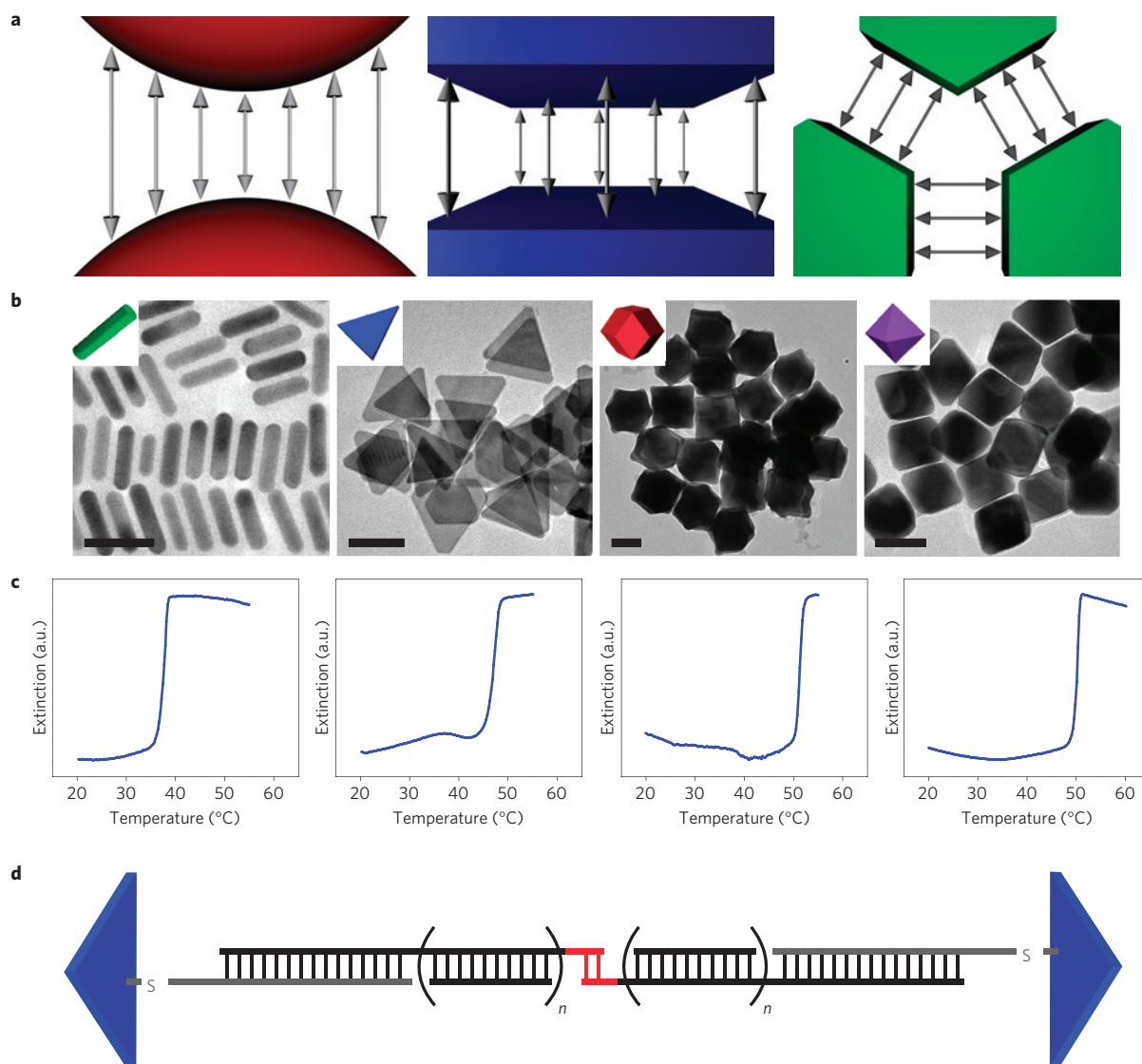


Figure 1 | Directional bonding interactions can be imparted to monodisperse, DNA-functionalized gold nanostructures through the introduction of shape anisotropy. **a**, The curved surfaces of spherical particles (left) cannot support the same number of idealized oligonucleotide interactions without DNA deformation as the flat, faceted surfaces of anisotropic nanostructures (middle). This feature allows for the shape of a nanostructure to more strongly dictate the structural details of the assembled superlattice it composes (right). **b**, Transmission electron microscopy images of (from left to right) rods, triangular prisms, rhombic dodecahedra and octahedra. The scale bars represent 50 nm. **c**, Extinction monitored at surface plasmon resonance maximum (from left to right: rods—800 nm, prisms—1,200 nm, rhombic dodecahedra—618 nm, octahedra—550 nm) as a function of temperature for DNA-functionalized anisotropic nanostructures assembled with linker oligonucleotides. The sharp melting transitions are indicative of a dense surface coverage of DNA. **d**, Schematic of the oligonucleotides used to assemble anisotropic nanostructures. Thiolated DNA strands (grey) anchored to the particle's surface were hybridized to linker DNA (black), which contained modular blocks of a repeated 40-base-pair sequence (labelled 'n', where n refers to the number of 40-base segments) and a short self-complementary (GCGC) recognition sequence (red) that induced particle assembly.

particle crystallization²⁸. Therefore, in all cases presented here, one can visually observe the initial formation of large, disordered aggregates and differentiate the subsequent ordering events using SAXS.

Gold nanorods were assembled using DNA linkers of varying lengths; on annealing, the resulting superlattices possessed long-range hexagonal symmetry (Fig. 2a,b, Table 1). Most crystals exhibited scattering peaks corresponding only to 2D ordering (Supplementary Figs S5, S6, S21). However, extended thermal annealing of some samples resulted in ordering between 2D sheets, with the resulting peaks indexing to a $P6_3/mmc$, hexagonal-close-packed, lattice. As nanorods were observed to order into 2D sheets in most samples studied, one can conclude that the particles favour interactions perpendicular to their long axis, demonstrating that the '1D' shape is directing their crystallization into primarily a

2D lattice, and these 2D lattices can subsequently reorganize into an ordered 3D structure. This was further probed through *in situ* monitoring of the crystallization process (Supplementary Fig. S22), wherein peaks corresponding to 2D order appear and begin to sharpen (indicating growth in crystal domain size) significantly before any peaks corresponding to 3D order appear.

The assembly of triangular nanoprisms was then investigated as an example of a '2D' nanostructure, wherein the length and width of a prism are an order of magnitude greater than its depth. One would expect the most dominant crystallization force to be face-to-face interactions between the predominantly 2D nanoprisms. Scattering patterns from superstructures of assembled prisms indicate a lamellar (or columnar) 1D arrangement of particles stacked in a face-to-face configuration (Fig. 2c,d). This is consistent with the

Table 1 | Summary of crystallization parameters for DNA-functionalized anisotropic nanoparticle superlattices.

	Nanoparticle dimensions (nm)	Lattice parameters (nm)	Average crystal domain sizes (nm)	Average no. unit cells/crystal
Rods	14 (w) x 55 (l)	34.3, 55.8, 77.9, 97.9, 110	1,270 ± 310	330 ± 210
	19 (w) x 52 (l)	34.3, 57.7, 77.6, 93.9, 113	1,180 ± 650	220 ± 120
Triangular prisms	60 (e) x 7 (w)	26.2, 48.3, 71.8, 94.3, 113	750 ± 230	14 ± 4
	95 (e) x 7 (w)	23.6, 48.6, 72.1, 94.9, 114	980 ± 400	18 ± 6
	140 (e) x 7 (w)	24.4, 48.9, 72.3, 93.3, 114	1,040 ± 510	19 ± 6
Rhombic dodecahedra	39 (e), 64 (d)	181, 201	2,550 ± 990	1,160 ± 810
	50 (e), 81 (d)	198, 220	1,780 ± 490	420 ± 120
Octahedra	59 (e), 83 (d)	110, 118 (bcc); 135, 159 (fcc)	1,510 ± 170	910 ± 470

Nanoparticle dimensions were obtained from transmission electron microscopy images and lattice parameters, domain size and unit cells per crystal were obtained from SAXS data (w—width, l—length, e—edge length, d—diameter). Calculations can be found in the Supplementary Information.

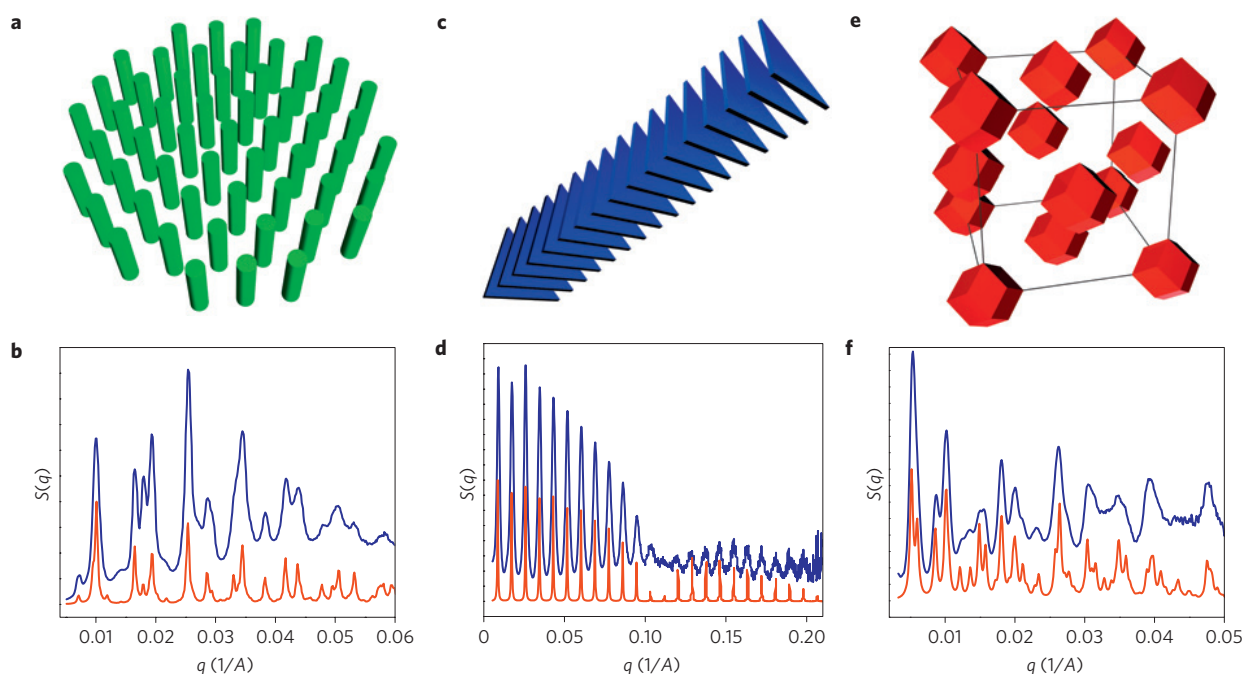


Figure 2 | SAXS characterization of anisotropic nanoparticle colloidal crystals. **a**, Schematic of a hexagonal 2D layer (additional layers omitted for clarity) in assemblies of gold nanorods. **b**, Experimental (blue) and simulated (red) SAXS patterns for gold nanorods (55 nm length, 14 nm diameter) assembled into a hexagonal-close-packed lattice with lattice constants of $a = 76.0$ nm and $c = 176.5$ nm. **c**, Schematic of the primarily 1D lamellar assemblies of gold triangular nanoprisms. **d**, Experimental (blue) and simulated (red) SAXS patterns for nanoprisms (95 nm edge length, 7 nm thickness) assembled into a columnar arrangement with a lattice spacing of 72.1 nm. **e**, Schematic of the 3D fcc assemblies of gold rhombic dodecahedra. The lines denote the fcc unit cell, not interparticle interactions. **f**, Experimental (blue) and simulated (red) SAXS patterns for rhombic dodecahedra (64 nm diameter) assembled into an fcc arrangement with a lattice constant of 201.4 nm.

previous observation (see above) that particles associate in a manner that maximizes hybridization interactions. Unlike the primarily 2D hexagonally packed nanorods, no long-range DNA-mediated ordering was observed between 1D stacks of prisms. Some crystals that underwent significant thermal annealing exhibited short-range order between nanoprism superlattices (Supplementary Fig. S23), but these scattering patterns could not be attributed to a well-defined 3D lattice. This lack of 3D ordering can be explained by the inherent thinness of the prisms (7 nm) and the relative rigidity of double-stranded DNA (persistence length of ~ 50 nm; ref. 29), resulting in very low DNA density along the side of a column. As the long axis of a 1D stack of prisms contains a relatively diffuse coating of DNA sticky ends, we project that hierarchical crystallization of these columns is not favourable

enough to produce 3D structures in the timescales monitored herein (see Supplementary Information for more detail).

A high degree of precision over the placement of prisms in 1D chains can be seen qualitatively by the large number of diffraction peaks present in the scattering pattern. Quantification of the rise per base pair (particle face-to-face distance divided by number of DNA bases) for three different particle sizes (edge lengths = 60, 95, 140 nm) and three different linker lengths (DNA lengths = 40.5, 63.5, 86.5 nm) yields a value of 0.281 ± 0.002 nm. This is a remarkable level of precision and programmability over the placement of nanomaterials along one dimension that would be difficult, if not impossible, to replicate by any lithographic or other directed-assembly method, illustrating one of the primary advantages of the DNA-directed crystallization methodology.

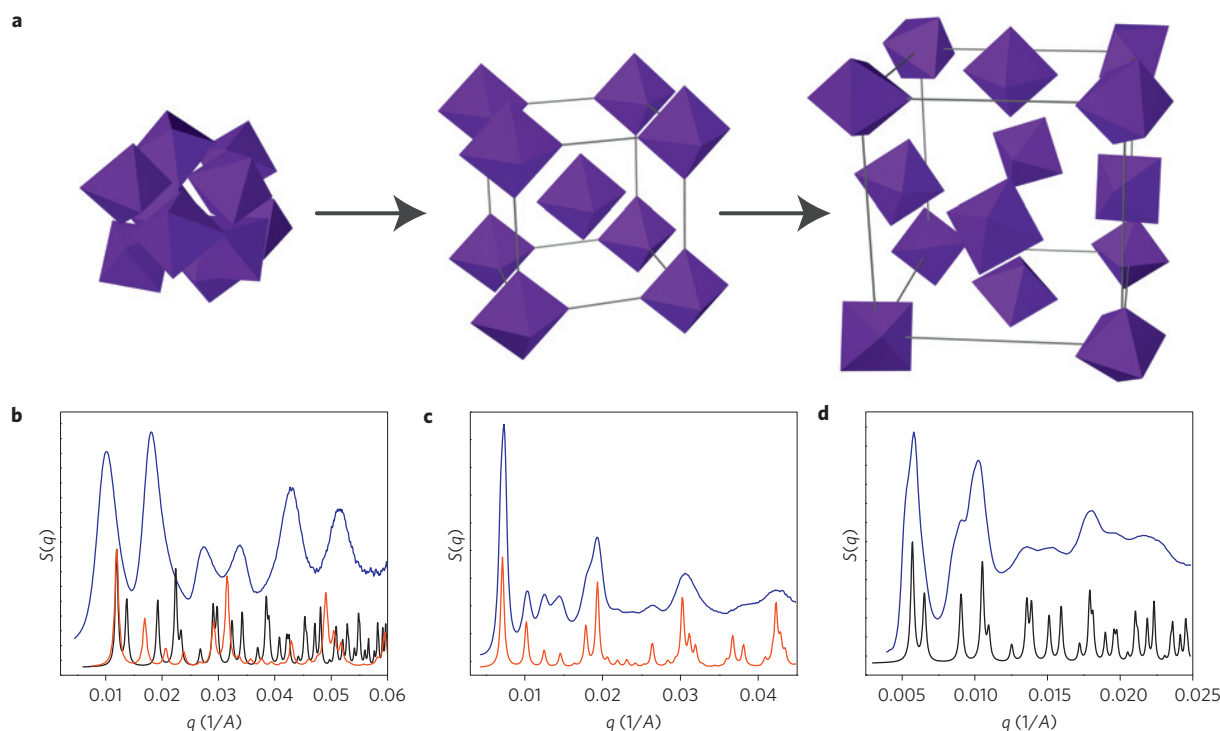


Figure 3 | Nanoparticle colloidal crystals undergo phase transformations as a function of DNA length. **a**, Schematic of disordered, bcc and fcc phases of crystallized octahedral nanoparticles, which are stable at short, intermediate and long DNA lengths, respectively. **b**, Experimental (blue) SAXS characterization of gold octahedra (59 nm edge length) assembled with short DNA (~15 nm) resulting in an interparticle distance of 76.8 nm. Simulated SAXS patterns for bcc (red) and fcc (grey) crystals with lattice parameters that would be expected given the length of the linking DNA strands demonstrate that the particles do not correlate with either lattice. Calculations and further explanation can be found in the Supplementary Information. **c**, Experimental (blue) and simulated (red) SAXS patterns for octahedra assembled with DNA linkers of an intermediate length (~45 nm) resulting in face-to-face orientational ordering within a bcc crystal with a lattice parameter of 118.4 nm. **d**, Experimental (blue) and simulated (grey) SAXS patterns for octahedra assembled with long DNA (~90 nm) resulting in no orientational ordering within an fcc crystal with a lattice parameter of 194.7 nm.

In accordance with the previous definitions of particle dimensionality (see above), a '3D' object would have no physical dimension significantly larger or smaller than the other two. The rhombic dodecahedron is an ideal particle to investigate the role of shape in 3D nanoparticle crystallization, as it naturally forms a face-centred-cubic (fcc) lattice with 100% packing efficiency, contrasted with previous fcc lattices of spherical particles^{3,23}, which exhibit a packing density of only ~74%. Unlike spheres, which interact in an isotropic fashion along a curved surface, maximum DNA interactions for the rhombic dodecahedron system would be obtained only when the particles associate face-to-face and are ordered in an fcc lattice with both positional and orientational order. Comparing the crystallization of rhombic dodecahedra to similarly sized spheres would give a good indication of how shape anisotropy affects positional and rotational order and crystal quality in the resulting colloidal superlattices.

The SAXS data confirm that the rhombic dodecahedra crystallize into fcc lattices and retain the lattice parameter programmability imparted by variations in DNA linker length (Fig. 2e,f, Supplementary Figs S10 and S11). Importantly, the lattices exhibit a significantly larger number of scattering peaks than fcc crystals consisting of similarly sized spherical particles²³, indicating greater positional order with respect to an ideal fcc lattice. Relative intensities of diffraction peaks correlate with modelled SAXS patterns for lattices wherein the rhombic dodecahedra retain orientational order (Supplementary Information, Figs S24–S29). This ordering occurs even when the hydrodynamic size of the 'DNA shell' is significantly larger than that of the particle, confirming that the rhombic dodecahedron shape does indeed have a strong influence on colloidal crystal formation. From these data, one can conclude

that the incorporation of shape anisotropy provides significant benefit to packing precision over the assembly of isotropic spheres.

It is important to note that the DNA linkers directing the crystallization process are not completely rigid. With increasing DNA length, one would expect the increasing flexibility of the DNA strands to change the sphericity of the DNA shell. Rhombic dodecahedra crystallized in fcc lattices retain their orientational order, indicating that the shape of their DNA shell is similar over all DNA lengths examined. Octahedra are another interesting class of particle worth probing in this manner. Experimentally and theoretically, octahedra pack most densely in lattices that do not maximize commensurate face-to-face interactions^{30–32}. Therefore, octahedral nanoparticles allow one to test the hypothesis that DNA-driven particle assembly and crystallization favours the structure that maximizes hybridization events and, in the case of anisotropic nanostructures, face-to-face interactions.

SAXS data demonstrate that the octahedra crystallize into a disordered lattice, a body-centred-cubic (bcc) lattice and an fcc lattice, with short, intermediate and long DNA lengths, respectively (Fig. 3a). With short DNA, only short-range order is observed—the corresponding scattering pattern does not index with either a bcc or fcc lattice, the two structures observed for longer DNA lengths (Fig. 3b). Although several possible lattices have been proposed for the dense packing of octahedra without DNA (refs 30–32), with short, inflexible DNA, none of these would produce a stable structure, according to the hypothesis, because they all exhibit severely limited face-to-face overlap (see Supplementary Information). At a DNA length of ~45 nm, however, the scattering peaks index to a bcc lattice; the intensities of these peaks are best fitted by a model that includes face-to-face orientational ordering between

octahedra (Fig. 3c). As the DNA is more flexible, the shape of the DNA shell may appear more like a truncated octahedron, which is able to maximize face-to-face interactions in a bcc arrangement (see Supplementary Information). At a DNA length of ~ 90 nm, the scattering pattern indexes to an fcc lattice, indicative of a particle that is more similar to a sphere than a well-defined octahedron (Fig. 3d). In this case, the intensities of the peaks indicate no orientational alignment of particles, as would be expected of a DNA shell that is approximately spherical. These data indicate that, at all DNA lengths, shape has a significant impact on the most stable structure, but, depending on DNA flexibility, the particle and the DNA have differing levels of importance in determining the anisotropy of the interactions between DNA-functionalized particles. Therefore, the interplay between the two components of this bionanoconjugate crystallization methodology provides a means to control the phase behaviour of a colloidal superlattice constructed from a given set of anisotropic nanostructure building blocks.

We have demonstrated that particle shape has a strong influence on the crystallization parameters of DNA-functionalized nanoparticles, affecting superlattice dimensionality, crystallographic symmetry and phase behaviour. Furthermore, the use of DNA as a programmable linker imparts the ability to tune the lattice parameters of the resulting crystals while retaining the shape directing effects of the nanoparticles within the limits of DNA flexibility. Moreover, this work is consistent with the conclusion that nanoparticle superlattices that can maximize interparticle DNA hybridization events will be the most stable structures. Such crystals may find use in applications that take advantage of the ability to tune the unique physical properties of these structures, such as plasmonic-based circuitry or waveguides, photonic bandgap materials and energy harvesting or storage materials, all of which exhibit unique emergent properties that are dependent on interparticle distance and crystal symmetry. In particular, the precision with which we can position particles is difficult to replicate using other assembly or lithographic techniques, indicating that this methodology provides a powerful means to realize these types of designer materials. Furthermore, we project that these results will enable fundamental insights into shape-directed hybridization effects and the influence of nanostructure valency on crystallographic parameters.

Received 6 May 2010; accepted 31 August 2010; published online 3 October 2010

References

- Mirkin, C. A., Letsinger, R. L., Mucic, R. C. & Storhoff, J. J. A DNA-based method for rationally assembling nanoparticles into macroscopic materials. *Nature* **382**, 607–609 (1996).
- Park, S.-J., Lazarides, A. A., Storhoff, J. J., Pesce, L. & Mirkin, C. A. The structural characterization of oligonucleotide-modified gold nanoparticle networks formed by DNA hybridization. *J. Phys. Chem. B* **108**, 12375–12380 (2004).
- Park, S. Y. *et al.* DNA-programmable nanoparticle crystallization. *Nature* **451**, 553–556 (2008).
- Nykypanchuk, D., Maye, M. M., van der Lelie, D. & Gang, O. DNA-guided crystallization of colloidal nanoparticles. *Nature* **451**, 549–552 (2008).
- Shevchenko, E. V., Talapin, D. V., Kotov, N. A., O'Brien, S. & Murray, C. B. Structural diversity in binary nanoparticle superlattices. *Nature* **439**, 55–59 (2006).
- Glotzer, S. C. & Solomon, M. J. Anisotropy of building blocks and their assembly into complex structures. *Nature Mater.* **6**, 557–562 (2007).
- Lapointe, C. P., Mason, T. G. & Smalyukh, I. I. Shape-controlled colloidal interactions in nematic liquid crystals. *Science* **326**, 1083–1086 (2009).
- Sacanna, S., Irvine, W. T. M., Chaikin, P. M. & Pine, D. J. Lock and key colloids. *Nature* **464**, 575–578 (2010).
- Zerrouki, D., Baudry, J., Pine, D., Chaikin, P. & Bibette, J. Chiral colloidal clusters. *Nature* **455**, 380–382 (2008).
- Srivastava, S. *et al.* Light-controlled self-assembly of semiconductor nanoparticles into twisted ribbons. *Science* **327**, 1355–1359 (2010).
- DeVries, G. A. *et al.* Divalent metal nanoparticles. *Science* **315**, 358–361 (2007).
- Liu, Q. *et al.* Self-alignment of plasmonic gold nanorods in reconfigurable anisotropic fluids for tunable bulk metamaterial applications. *Nano Lett.* **10**, 1347–1353 (2010).

- Ming, T. *et al.* Ordered gold nanostructure assemblies formed by droplet evaporation. *Angew. Chem. Int. Edn* **120**, 9831–9836 (2008).
- Tao, A., Sinsermsuksakul, P. & Yang, P. Tunable plasmonic lattices of silver nanocrystals. *Nature Nanotechnol.* **2**, 435–440 (2007).
- Alivisatos, A. P. *et al.* Organization of 'nanocrystal molecules' using DNA. *Nature* **382**, 609–611 (1996).
- Wei, Y., Bishop, Kyle J. M., Kim, J., Soh, S. & Grzybowski, B. A. Making use of bond strength and steric hindrance in nanoscale 'Synthesis'. *Angew. Chem. Int. Edn* **121**, 9641–9644 (2009).
- Li, M., Schnablegger, H. & Mann, S. Coupled synthesis and self-assembly of nanoparticles to give structures with controlled organization. *Nature* **402**, 393–395 (1999).
- Stebe, K. J., Lewandowski, E. & Ghosh, M. Oriented assembly of metamaterials. *Science* **325**, 159–160 (2009).
- Nie, Z. *et al.* Self-assembly of metal-polymer analogues of amphiphilic triblock copolymers. *Nature Mater.* **6**, 609–614 (2007).
- Li, F., Yoo, W. C., Beernink, M. B. & Stein, A. Site-specific functionalization of anisotropic nanoparticles: From colloidal atoms to colloidal molecules. *J. Am. Chem. Soc.* **131**, 18548–18555 (2009).
- Millstone, J. E. *et al.* DNA-gold triangular nanoprism conjugates. *Small* **4**, 2176–2180 (2008).
- Zhang, Z. & Glotzer, S. C. Self-assembly of patchy particles. *Nano Lett.* **4**, 1407–1413 (2004).
- Macfarlane, R. J. *et al.* Establishing the design rules for DNA-mediated programmable colloidal crystallization. *Angew. Chem. Int. Edn* **49**, 4589–4592 (2010).
- Millstone, J. E. *et al.* Observation of a quadrupole plasmon mode for a colloidal solution of gold nanoprisms. *J. Am. Chem. Soc.* **127**, 5312–5313 (2005).
- Nikoobakht, B. & El-Sayed, M. A. Preparation and growth mechanism of gold nanorods (NRs) using seed-mediated growth method. *Chem. Mater.* **15**, 1957–1962 (2003).
- Niu, W. *et al.* Selective synthesis of single-crystalline rhombic dodecahedral, octahedral, and cubic gold nanocrystals. *J. Am. Chem. Soc.* **131**, 697–703 (2008).
- Jin, R., Wu, G., Li, Z., Mirkin, C. A. & Schatz, G. C. What controls the melting properties of DNA-linked gold nanoparticle assemblies? *J. Am. Chem. Soc.* **125**, 1643–1654 (2003).
- Macfarlane, R. J. *et al.* Assembly and organization processes in DNA-directed colloidal crystallization. *Proc. Natl Acad. Sci. USA* **106**, 10493–10498 (2009).
- Rivetti, C., Walker, C. & Bustamante, C. Polymer chain statistics and conformational analysis of DNA molecules with bends or sections of different flexibility. *J. Mol. Biol.* **280**, 41–59 (1998).
- Lu, W. *et al.* Super crystal structures of octahedral c-In₂O₃ nanocrystals. *J. Am. Chem. Soc.* **130**, 6983–6991 (2008).
- Xie, S. *et al.* Supercrystals from crystallization of octahedral MnO nanocrystals. *J. Phys. Chem. C* **113**, 19107–19111 (2009).
- Torquato, S. & Jiao, Y. Dense packings of the Platonic and Archimedean solids. *Nature* **460**, 876–879 (2009).

Acknowledgements

C.A.M. acknowledges the NSF-NSEC and the AFOSR for grant support, and the DOE Office (Award No. DE-SC0000989) for support through the NU Nonequilibrium Energy Research Center. He is also grateful for an NSFE Fellowship from the DoD. M.R.J. acknowledges Northwestern University for a Ryan Fellowship and the NSF for a Graduate Research Fellowship. R.J.M. acknowledges Northwestern University for a Ryan Fellowship. K.L.Y. acknowledges the NSF and the NDSEG for Graduate Research Fellowships. Portions of this work were carried out at the DuPont-Northwestern-Dow Collaborative Access Team (DND-CAT) beamline located at Sector 5 of the Advanced Photon Source (APS). DND-CAT is supported by E.I. DuPont de Nemours & Co., The Dow Chemical Company and the State of Illinois. Use of the APS was supported by US Department of Energy, Office of Science, Office of Basic Energy Sciences, under Contract No. DE-AC02-06CH11357. The transmission electron microscope work was carried out in the EPIC facility of NUANCE Center at Northwestern University. NUANCE Center is supported by NSF-NSEC, NSF-MRSEC, Keck Foundation, the State of Illinois and Northwestern University. Ultrathin sectioning was carried out at the Northwestern University Biological Imaging Facility supported by the NU Office for Research.

Author contributions

M.R.J. and R.J.M. designed the systems, prepared the materials, collected and analysed the data and wrote the manuscript. B.L. analysed the data, carried out simulations of nanoparticle superlattices and wrote the manuscript. J.Z., K.L.Y. and A.J.S. collected data. C.A.M. designed the systems and wrote the manuscript.

Additional information

The authors declare no competing financial interests. Supplementary information accompanies this paper on www.nature.com/naturematerials. Reprints and permissions information is available online at <http://npg.nature.com/reprintsandpermissions>. Correspondence and requests for materials should be addressed to C.A.M.